

Chapter 7

Development of Lightning Hazard Map for Fire Danger Assessment Over Mountainous Protected Area Using Geospatial Technology



Dipuo Olga Mofokeng, Adeyemi Olusola, and Samuel Adelabu

Abstract Lightning is regarded as a leading cause of fatalities, injuries, property damages, and interruptions to businesses. As against some other tropical countries, especially around the equator in Africa and South America, South Africa does not experience as much lightning activity; however, it is still considered a lightning-prone country. With the advent of remote-sensing technology and its capabilities, the world can detect nearly all lightning strikes in real-time with the ability to also geolocate the strike with high temporal and spatial accuracy. This study aims to advance the understanding of the geography of CG lightning activity in South Africa through the application of geospatial technology. Using spatial analysis techniques, this research evaluated 11-year lightning data (2007–2017) to develop a lightning hazard map for Golden Gate Highlands National Park. The monthly strike count of lightning increases from the minimum value in July (0.08%) and displays a peak in December (23.80%). The average diurnal variation (2007–2017) suggests that lightning is more prevalent in terms of occurrence from 14:00 to 18:00 SAST with two clear maxima at 15:00 SAST and 17:00 SAST. The lowest lightning activity is during the morning hours at 05:00 and 06:00 SAST, and yet again at hour 08:00 SAST. The average diurnal variation (2007–2017) suggests that lightning is more prevalent in terms of occurrence from 14:00 to 18:00 SAST with two clear maxima at 15:00 SAST and 17:00 SAST. The lowest lightning activity is during the morning hours at 05:00 and 06:00 SAST, and yet again at hour 08:00 SAST.

D. O. Mofokeng (✉)

Department of Geography, Afromontane Research Units (ARU), University of the Free State, Phuthaditjhaba, Free State, South Africa

A. Olusola · S. Adelabu

Department of Geography, University of the Free State, Bloemfontein Campus, South Africa

Spatial autocorrelation analysis revealed that the clustering of lightning strikes at the park is at the distance of about 1.2 km. This connotes that strikes clustered with other strikes are not likely to strike an individual specific location from centre of cluster of strikes much beyond a circle with a radius of 1.2 km.

Keywords Lightning · Spatial Statistics techniques · Remote Sensing · Fire Danger Assessment

7.1 Introduction

Lightning as an activity most likely predates human existence (Gijben, 2012, Rakov and Uman, 2003) and even a critical meteorological phenomenon. Lightning is regarded as a leading cause of fatalities, injuries, property damages, and interruptions to businesses (Cha et al., 2017, Gijben et al., 2017). By definition, lightning can be described as the release of static electricity in the sky or between the clouds and the ground (Gijben, 2012, Rakov and Uman, 2003). On a global scale, lightning is responsible for not more than 24,000 deaths and 240,000 injuries on an annual basis (Blumenthal et al., 2012). From Earth Observation Satellites (EOS), about 39–49 lightning flashes are captured around the globe per second. This is translated to about 1.4 billion flashes per day on a Cloud-to-Ground (CG) scenario (Christian et al., 2003, Gijben et al., 2017).

As against some other tropical countries, especially around the equator in Africa and South America, South Africa does not experience as much lightning activity; however, it is still considered a lightning-prone country (Bhavika, 2007, Gijben, 2012). Yearly death rates from lightning in South Africa is 6.3 per million of the population, which is 15 times more than the global average (Gill, 2009). This figure is presumed to be underestimated per actual mortality rate. This underestimation is likely to be because lightning deaths are not rigidly reported in rural areas (Gijben et al., 2017). As a natural ignition source for global fire, lightning activities were recently operationalized as one of the driving factors in fire danger or risk modelling (Chuvienco et al., 2014, 2010, Eskandari and Chuvienco, 2015, Huang et al., 2015). According to Cha et al. (2017), an average of 816 fires were ignited by lightning each year globally.

During 2005, lightning fire burnt a large area of fynbos and commercial timber plantation in Tsitsikamma, Western Cape Province of South Africa (Durrheim, 2010). According to the Council for Scientific and Industrial Research (CSIR) report on the Elandskraal fire that ravaged approximately 9440 hectares, it was revealed that the positive lightning strike observed on the 22 March 2017 was responsible for the fire which started on the 07 June 2017 (Frost et al., 2018).

With the advent of remote-sensing technology and its capabilities, the world can detect nearly all lightning strikes in real-time with the ability to also geolocate the strike with high temporal and spatial accuracy. Numerous studies have focused on understanding lightning activities in many countries using different lightning

location systems (Christian et al., 2003; Rakov and Uman, 2003; Kigotsi et al., 2018). Most of the lightning systems detect electromagnetic reading using Time of Arrival (ToA) and Magnetic Direction Findings (MDF) methods or a combination of ToA and MDF. A summary of literature relating to the methods can be found in (Gill, 2009). These systems are either ground-based or satellite lightning sensors. The latter detects lightning from space through the earth-orbiting satellite which either detects light or electromagnetic waves from lightning discharge (Rakov and Uman, 2003). The well-known satellite-lightning sensors include National Aeronautical & Space Administration (NASA) Optical Transient Detector (OTD) and Lightning Imaging Sensors (LIS) on-board the Tropical Rainfall Measuring Mission (TRMM) (1997–2014) (Christian et al., 2003, Kigotsi et al., 2018). Formerly, sensors which detect electromagnetic pulse in very low frequency (VLF) or low frequency (LF) include regional Lightning Detection Network (LDN) such as United States of America National Lightning Detection Network (USA NLDN) and Southern African Lightning Detection Network (SALDN) in South Africa. Global LDN includes World Wide Lightning Location Network (WWLLN) and the Global Lightning datasets (Kigotsi et al., 2018).

The spatio-temporal lightning flash density and occurrence have been investigated in the United States (Bentley and Stallins, 2005); Canada (Cha et al., 2017), Europe (Anderson and Klugmann, 2014), Mediterranean (Price and Federmesser, 2006), India (Dewan et al., 2018), Africa (Kigotsi et al., 2018, Mayet et al., 2016) at the global scale (Cecil et al., 2014, Christian et al., 2003). According to Evert and Schulze (2005), studies on lightning have been in existence for about eight decades. However, in the past couple of years, there has been tremendous growth in South Africa as a result of the introduction of the National System (see Gill, 2009). Gill (2009) was the first to utilize the 2006 SALDN data in the development of the climatology of South Africa. This was later updated by Gijben (2012) using the 2006–2010 dataset. Recently, Evert and Gijben (2017) utilized the 2006–2017 SALDN data to update the national lightning flash density map over South Africa. In their study, Evert and Gijben (2017) observed that the highest flash density occurs along the eastern escarpment of the country with values exceeding 15 flashes $\text{km}^{-2} \text{yr}^{-1}$.

Despite the availability of geo-coordinated lightning data, most CG lightning studies found within the country (South Africa) typically only focus on visualizing the distribution of CG lightning activity as a flash density for the simple purpose of identifying areas of high flash density rate. These forms of studies often do little in explaining the observed spatial patterns of flash density. Furthermore, based on the uniqueness of the country's physiography, there are landscapes across the country that are unique to lightning activities, such as montane environments. Montane environments within South Africa are unique, in that they serve as places of water towers for South Africa and some neighbouring countries, also these areas preserve very unique grasslands that are endemic to South Africa and of global interest. Also, montane environments in South Africa are witnessing the impact of the changing climate through the emergence of invasive species and incessant lightning strikes. Therefore, this study aims to advance the understanding of the geography of CG

lightning activity in South Africa through the application of geospatial technology. Using spatial analysis techniques, this research evaluated 11-year lightning data (2007–2017) to develop a lightning hazard map for Golden Gate Highlands National Park by examining the statistical spatial and temporal patterns of lightning activity of Golden Gate Highlands National Park and their relationship with environmental characteristics, namely, elevation, slope, aspect, fire scars, and the vegetation type.

7.2 Material and Methods

7.2.1 Study Area

As a protected montane area, the Golden Gate Highland National Park (GGHNP) lies between 1657 m and 2797 m above sea level north-eastern of the Free State Province in South Africa (South African National Parks, 2013) (Fig. 7.1). The park is a unique Grassland Biome in South Africa and is situated in the summer rainfall region. The rainfall here is characterized by seasonal stretching from September to April with a mean annual value between 1800 mm and 2000 mm. The area is categorized as a dry sub-humid region. Summers are temperate with mean temperature (13 °C–26 °C) and winters are cold with mean temperature (1 °C–15 °C). In essence,

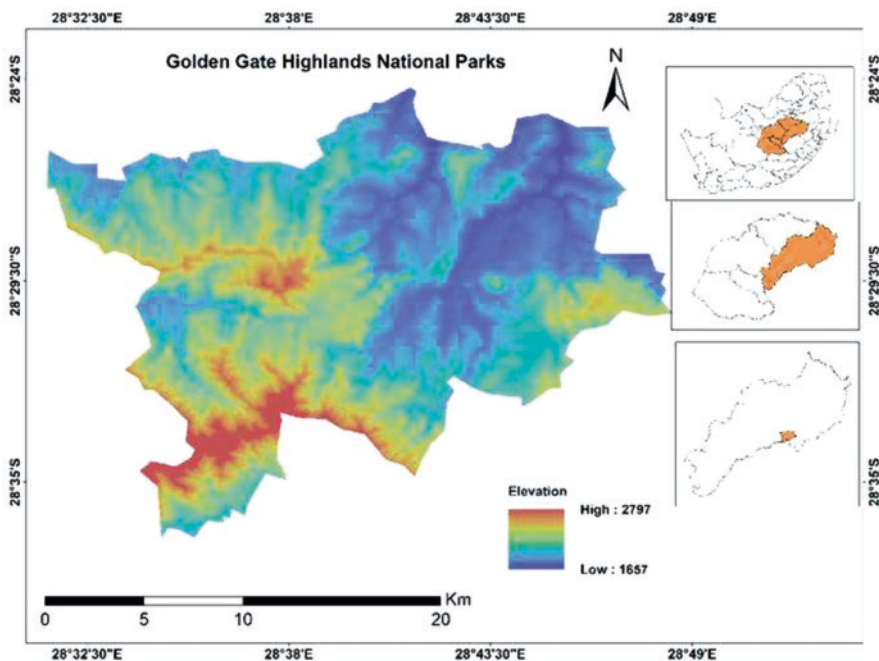


Fig. 7.1 Location of the study area (GGHNP)

the fire season starts in May and lasts till September. Despite numerous fire mitigation and management strategies (Strydom and Savage, 2016), this region is still highly vulnerable to wildfire which is in part due to its rugged terrain. On average, the park has lost 6809 ha of vegetation to fire accounting for 20% of the area (Govender, 2011).

7.2.2 *Material*

7.2.2.1 CG Lightning Data

CG lightning data was acquired from the Southern African Lightning Detection Network (SALDN) of the South African Weather Services (SAWS). The SALDN became operational in 2005 and underwent a series of upgrades. From 2015, the network consisted of 25 Vaisala CG lightning sensors that can detect all cloud-to-ground lightning discharges with a 90% efficiency measure (Evert and Gijben, 2017). The SALDN is capable of detecting lightning with a location accuracy of ~0.5 km (500 m) covering all of South Africa, Lesotho, and Swaziland (Bhavika, 2007, Evert and Gijben, 2017, Gijben et al., 2017). The network records lightning events chronologically. The attribute information of each lightning strike is recorded including date and time, latitude, longitude, peak current with negative(−) or positive (+) polarity, major and minor ellipsoid angle, and the number of direction finders that sensed the event (Bhavika, 2007). As recommended by International Electrotechnical Commission Standards (IEC 62858), lightning data for at least 10 years is required to ensure that short-term scale variation in lightning parameters due to a variety of meteorological oscillations are accounted for (Javor et al., 2018). Therefore, in this study, lightning strike data for 11 years from January 2007 to December 2017 was utilized.

7.2.2.2 Terrain Elevation, Slope, and Aspect

Advanced Spaceborne Thermal Emission and Reflection Radiometer-Digital Elevation Model (ASTER-DEM) data at 30 meters freely obtained from USGS EarthExplorer (<http://earthexplorer.usg.gov>) was used for retrieval of elevation, aspect, and slope values. These values were selected due to its known role of orographic lifting to the enhancement of convection and consequently to lightning (Kotroni & Lagouvardos, 2008).

7.2.2.3 Vegetation Type

Vegetation plays a pivot role in the universal climatic variation together with the convective growth and lightning activity (Dissing and Verbyla, 2003; Mushtaq et al., 2018). Vegetation type of GGHNP was attained from Fire Ecology Department, South Africa National Park, in the polygon shapefile providing GIS coverage that shows vegetation types in community and habitat.

7.2.2.4 Historical Fire

Historical fire scar/spot data was received from the Fire Ecology and Biogeochemistry Department, South Africa National Parks, with their geographical coordinates in polygon shapefile format. The significance of these data in lightning activity is that a possible-induced thunderstorm can be conceived from all sides of fire scars (Kilinc and Beringer, 2007).

7.2.3 Methods

Lightning data was provided in a formatted text (.csv) that was first parsed and saved in a spreadsheet and then converted into a point vector layer in a GIS environment using Microsoft Excel and ArcMap 10.2. software, respectively. The georeference UTM Zone 35S was used as the projection. A Clip Tool was employed to extract the study area. Databases of lightning activity by year, monthly, and hourly were then created by using the Select by Attributes tool.

7.2.3.1 Temporal Distribution of Lightning Strikes Activity

Lightning strikes counts were analysed to explore temporal patterns of lightning activities over GGHNP. Annually, monthly, seasonal, and diurnal distributions were calculated with the summation of counts for respective periods. To evaluate the influence of season on lightning activity, monthly data was summarized according to four seasons: summer (Dec, Jan, Feb), autumn (March, April, May), winter (June, July & August), and spring (Sept, Oct, Nov). For diurnal, a series of graphs and tables were created using Excel to visualize the temporal distribution of lightning activity of the park.

7.2.3.2 Spatial Distribution of Lightning Strikes Activity

To capture the spatio-temporal distribution of lightning activity, maps for visualization showing the individual CG lightning strikes as points and density were created. In this study, the Hex binning analysis was employed. This analysis helps in aggregating spatially lightning strike data. The reason here is that the Hex binning as used in this study will help to spatially aggregate the dataset (lightning strike) in a hexagonal manner. The assumption stems from studies (Carr et al., 1992; Genton et al., 2006) that have posited that hexagons are visually appealing and have better symmetry of nearest neighbour than square or rectangular bins. The hex grid (100 m) for each of the dataset (lightning) were created using MMQGIS plugin version 2018.1.2 and the lightning data was spatially joined to the hex grid using the join by location attribute in QGIS 2.18.5. The lightning flash density attribute was added to the new feature table and calculated using the Field Calculator tool by dividing the 'count' by cell area and then by the number of years spanning the dataset resulting in a count per km² per year (Ng).

Hot Spot Analysis was employed to determine whether or not there is clustering and also to measure the degree of spatial autocorrelation of CG lightning in the study area. Hot Spot Analysis was performed using lightning strikes density data as an input. Several analyses or processes precede hotspot analysis. First, we determined the specific threshold distance or distance band for neighbouring feature, which is called neighbourhood. The neighbourhood consists of features that are analysed together to assess local clustering and this is made possible through the use of a threshold distant band (TDB). To determine the TDB, the Incremental Spatial Autocorrelation (ISA) tool in ArcGIS was conducted.

ISA is a measure of spatial autocorrelation. The Z-score here depicts the spatial clustering intensity and statistically significant peak z-score indicates where spatial processes promoting clustering are most pronounced. These peak distances were used to determine a distance band or threshold distance band for hot spot analysis using Getis–Ord G_i^* (ArcGIS, 2013, Cha et al., 2017).

Furthermore, Incremental Spatial Autocorrelation calculates Global Moran I. Moran's I is a measure of the correlation where negative correlation indicates the dispersion of similar values, positive correlation indicates clustering of similar values (either high or low), and zero correlation indicates complete spatial randomness. It informs us whether a set of features is clustered, dispersed, or random. It is based on spatial covariation divided by total variation as shown in Eq. 7.1 (Amrhein, 2017, Moran, 1950).

$$I = \frac{n \sum_{j=1}^n \sum_{j=1}^n W_{ij} (y_i - y)(y_j - y)}{\left(\sum_{i=1}^n (y_i - y)^2 \left(\sum_{i=1}^n \sum_{j=1}^n W_{ij} \right) \right)} \quad (7.1)$$

From Eq. (7.1), n is the total number of features, w_{ij} is the spatial weight matrix between feature i and j , the variable y is the features attribute value.

Values for Moran’s I range from -1 (dispersion) to $+1$ (clustered). A Z-score and p-value are also calculated for Moran’s I statistic. For statistically significant positive Z-scores, the null hypothesis of spatial randomness is rejected, and the high and low values in the dataset are considered to be more clustered than expected. For statistically significant negative Z-score, the spatial distribution of high and low values is considered dispersed and the null hypothesis is rejected (Amrhein, 2017, Moran, 1950). Results were represented in the form of line graphs of Moran I and Z-score vs distance.

To explain a spatial pattern of the CG lightning strike density, hotspot analysis was eventually performed using Hot Spot Analysis *Getis-Ord G_i^** Tool of ArcMap. *Getis-Ord G_i^** evaluates the spatial correlation from a local scale perspective. The G_i^* as a statistic helps in determining areas of high and low clusters by looking at local averages to global averages. The G_i^* statistic ranges in values from -3 to $+3$ and is calculated for each feature and produces a Z-score indicating the intensity of the high or low clustering with respect to its neighbourhood depending on the sign of Z-score. A statistically significant ‘hot spot’ is one where a feature with high value is surrounded by other features with high values (positive Z-score). Likewise, a ‘cold spot’ is one where a feature with low value is surrounded by other features with low values (ArcGIS, 2013, Cha et al., 2017, Getis and Ord, 1992). The G_i^* is calculated using Eq. 7.2.

$$G_i^* = \frac{\sum_{j=1}^n w_{i,j} x_j - X \sum_{j=1}^n w_{i,j}}{S \sqrt{\sum_{j=1}^n x_j^2 - (X)^2}} \tag{7.2}$$

where x_j is the attribute value for feature j , $w_{i,j}$ is the spatial weight between i and j , and n is equal to the total number of features. Also, X and S are shown in Eqs. 7.3 and 7.4, respectively.

$$X = \sum_{j=1}^n x_j \tag{7.3}$$

$$S = \sqrt{\sum_{j=1}^n x_j^2 - (X)^2} \tag{7.4}$$

7.3 Development of Lightning Hazard Map

For the spatial distribution of Lightning Hazard Map (LHM), the Inverse Distance Weighted (IDW) technique of ArcMap 10.2 was employed. LHM was developed from the Z-score of the Hot Spot Analysis. The output of the IDW was normalized to range between 0 and 1 using the Raster normalization tool (ArcGIS), while the Reclass tool was used to stratify the entire data layer into five classes based on lightning potential risk of lightning activities guided by previous researches. These classes are categorized as follows: almost danger-free (0–0.2), minimal danger (0.2–0.35); moderate danger (0.35–0.50); severe danger (0.50–0.75); and extreme Danger (0.75–1).

7.3.1 *Relationship of Lightning Hazard Map with Topography (Elevation, Slope, Aspects, Vegetation Types, and Fire Scar)*

Regression analysis was undertaken to explore the relationship of LHM with terrain parameters, (elevation, slope, and aspect), vegetation types, and fire scars. Statistical analysis of the data, namely, Coefficient, Probability or Robust Probability, and Variance Inflation Factor (VIF), as well as t-test were used to assess each variable. In preparing the data for statistical analysis, the study area elevation data was prepared using methods by Adelabu et al. (2018). Slope and aspect were calculated using the Surface Tool. All raster layers were converted into vector layers (polygons) to align with vegetation types and fire scar layers and resampled to 1000 m. All six (6) layers were overlaid using the Spatial Join Tool of ArcMap. Regression analysis was performed using Ordinary Least Squares (OLS) Modelling spatial relationship Tool of ArcMap 10.2 software. The diagnostic results were displayed in the form of a table.

7.4 Results

7.4.1 *CG Lightning Strike Events and Density Maps*

Within the GGHNP, a total of 114,720 lightning strikes were recorded between January 2007 and December 2017. About 94.86% were of negative polarity and 5.14% of positive polarity. In general, most of the previous studies showed a similar pattern of positive polarity accounting for less than 10% of total CG activities (Dewan et al., 2018). Since the CG lightning point event map is difficult to visually interpret, a lightning flash density map on the hexagon polygon grid for the entire 11-year period is displayed in Fig. 7.2. The map showed that the density of lightning

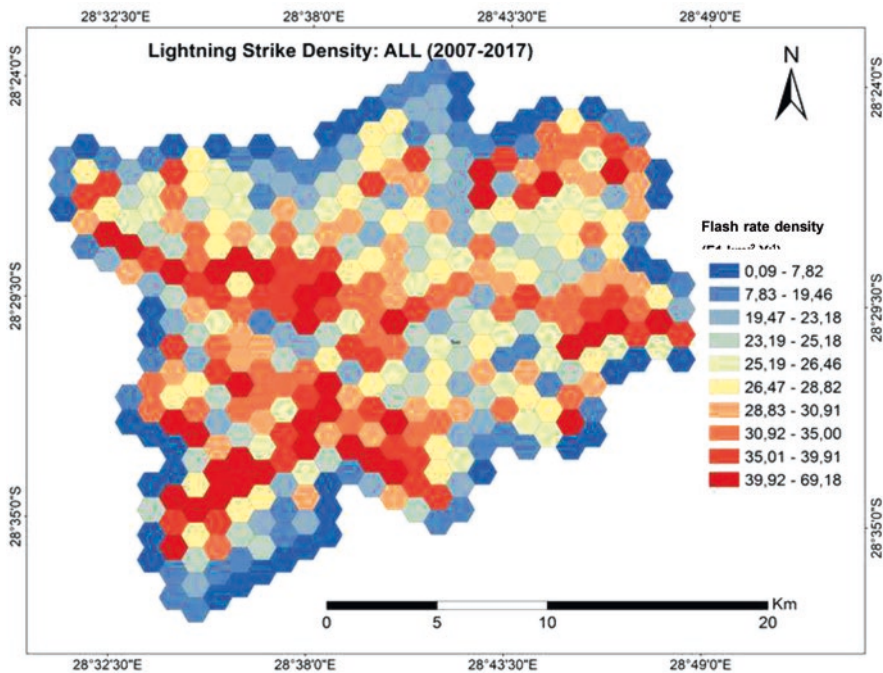


Fig. 7.2 Map depicting the spatial density of CG lightning flashes within GGHNP between 2007 and 2018. Lightning density (Ng) displayed the number of CG lightning events per km² per year

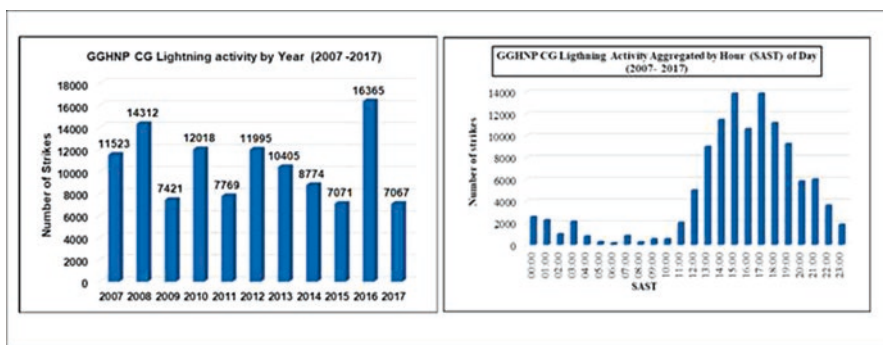


Fig. 7.3 Graph of lightning events by year and hour

strikes is not uniform throughout the park. Areas of high density (in red) can be seen throughout the park. These observed variations in the CG lightning pattern follow the topography of GGHNP. The highest density was prominent at a highly elevated area within the park.

7.4.2 Temporal Analysis

From Fig. 7.3, it can be observed that the GGHNP experienced the highest number of lightning events during 2016 (16,365). The distribution shows that the years 2015 (7071 events) and 2017 (7067 events) witnessed the lowest number of individual lightning strikes in the park. Based on the inter-annual variability (Fig. 7.3 and Table 7.1), there is a possibility that the occurrence of these strikes is related to a large-scale climate phenomenon, such as the ElNino Southern Oscillation (ENSO) and the Southern Annular Mode (SAM) (Dowdy, 2016, Guha et al., 2017, Mariani et al., 2016). However, there is still the need to carefully unravel this relationship using standard climatic procedures.

Fig. 7.4 shows the seasonal variation of lightning strikes over the GGHNP for the period between 2007 and 2018. It was evident that maximum lightning strikes were observed in summer. The decrease of lightning activity observed on the onset of autumn to the winter season is consistent with the results of (Gill, 2009). Gill (2009) also observed a shift in lightning activity with the change in season in South Africa. Regularly in summer, a surface trough (an elongated area with relatively low pressure values when reduced to sea level) associated with the deep intrusion of well-defined easterly wave that will result in the development of a line of convection extending from northwest towards the southeast over the country. Such line thunderstorms are well organized and moved from west to east bringing rain and accompanied lightning to the most of the Free State province (Gill, 2009). Low lightning activity in the winter season could be attributed to the less vegetation cover and more bare-ground. The study by Kotroni and Lagouvardos (2008) revealed that over a bare ground, the lightning yield is low. Changes in the surface temperature from minimum in winter followed by maximum on the onset of springs may lead to fluctuation of lightning activity. Moreover, high lightning activity in summer could be attributed to cloud cover during late springs.

Table 7.1 Percentage of lightning strikes count by month and season between 2007 and 2017

Month	Percentage	Season	Percentage
Dec	23.80%	Summer	56.26%
Jan	17.57%		
Feb	14.89%		
Mar	10.71%	Autumn	14.22%
Apr	2.82%		
May	0.69%		
Jun	0.47%	Winter	0.68%
Jul	0.08%		
Aug	0.13%		
Sep	1.90%	Spring	28.84%
Oct	13.38%		
Nov	13,56%		

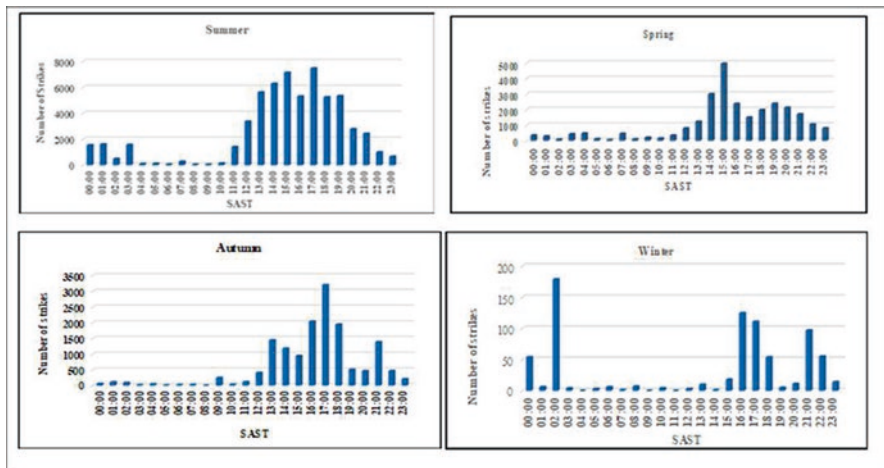


Fig. 7.4 Seasonal variation lightning strikes over GGHP

In addition, Fig. 7.4 illustrates the diurnal variation of lightning activity on a seasonal basis. It revealed that majority of lightning activity occurred in the afternoon to the early evening across all four seasons. The diurnal pattern described the influence of solar radiation on the development of thunderstorms. The observed afternoon peak in lightning activity correlates to the peak in solar radiation and subsequently high energy levels during this time of the day (Bhavika, 2007). Gill (2009) demonstrated that heat-generated, isolated, or scattered thunderstorm activity is also common in the late afternoon. However, an abnormal observation was made during winter season with peak in early hours of the morning (02:00). This diurnal pattern indicated that winter lightning is not sensitive to solar heating, and thus frontal activity is the dominant factor influencing thunderstorm development in this season (Bhavika, 2007).

7.5 Spatial Pattern Analysis

7.5.1 Global Moran I

Output from Moran I analysis on the monthly scale, as depicted in Fig. 7.5a, revealed that the Moran I values are greater than 0 ranging from 0.01 to 0.49 throughout the year, with the exception of July. This indicates positive spatial autocorrelation of clustering of either high or low values of CG lightning density. However, the Moran I value of July is smaller than 1 indicating that the spatial pattern is randomly distributed. In winter months (June, August, and September), Moran I values range from 0.01 to 0.07, which reveals that spatial pattern is close to the random distribution pattern of CG lightning density. The z-score values are above zero (see

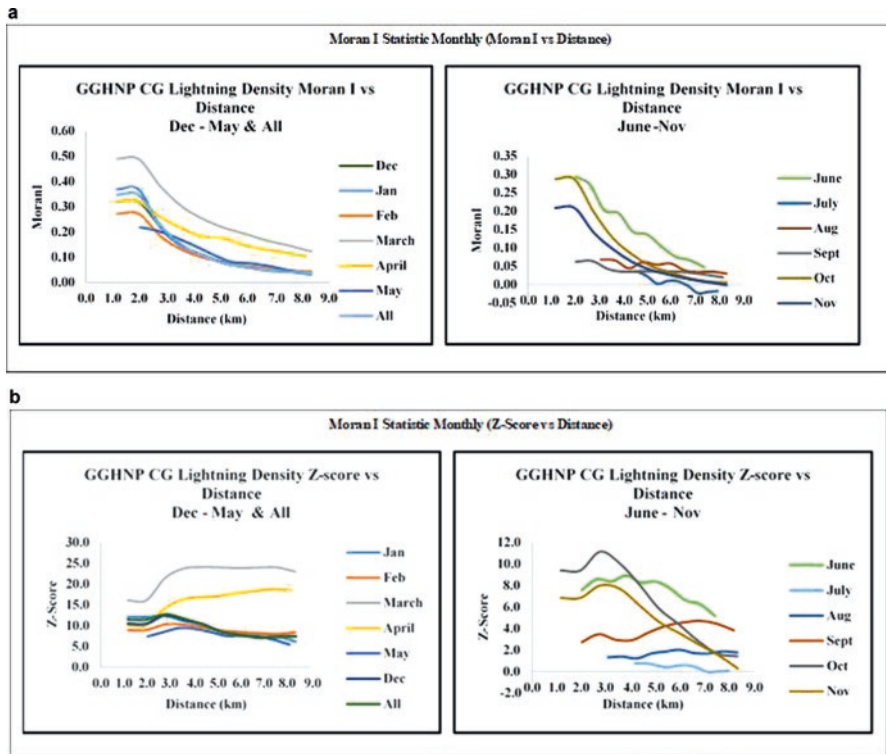


Fig. 7.5 Global Moran I statistic results for monthly data (a) Moran I vs Distance, (b) Z-score vs Distance

Fig. 7.5b) and observed p-values are low, therefore, the spatial pattern is statistically significant and rejected the null hypothesis that lightning density is randomly distributed except in the month of July. The CG lightning density and the Moran I curves show the bias of lightning density with distance. From Fig. 7.5a, b, the CG lightning density shows a persistent decrease with distance for afternoon and evening hours ranging from 0.00 to 0.48 at 1.2 km to values less than 0.0 at 8.3 km. From Fig. 7.5, it can be posited that the spatial distribution of lightning density within the protected area is clustered at a distance of about 1.2 km which becomes closer to random as the neighbourhood distance increases. On the other hand, the Moran I curve for late morning hours suggests a random pattern since the morning hours is less than zero and negative for 06:00 SAST and 09:00 SAST (Fig. 7.6a).

From Fig. 7.6b, the observed Z-score ($Z > 0$ and positive) curves for early morning, afternoon, and evening hours are above zero and are positive signalling a positive spatial auto-correlation and an indication of a significant clustered pattern ($p < 0.5$). Based on Fig. 7.6b, the Z-score ($Z < 0$ and negative) for late morning hours 06:00 and 08:00 SAST suggests a negative non-significant spatial correlation, hence, lightning activities within GGHNP during 06:00 and 08:00 are likely to be random.

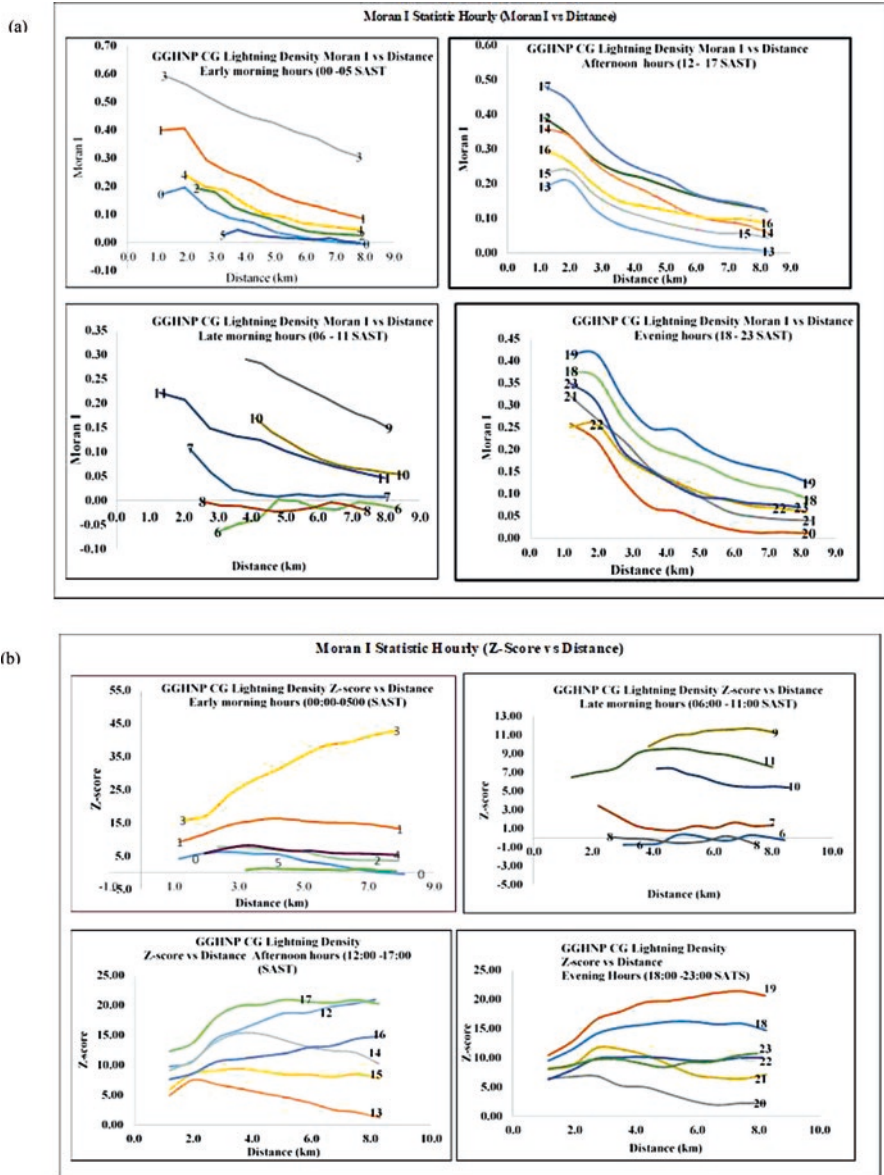


Fig. 7.6 Global Moran I statistic diurnal data (a) Moran I vs Distance, (b) Z-score vs Distance

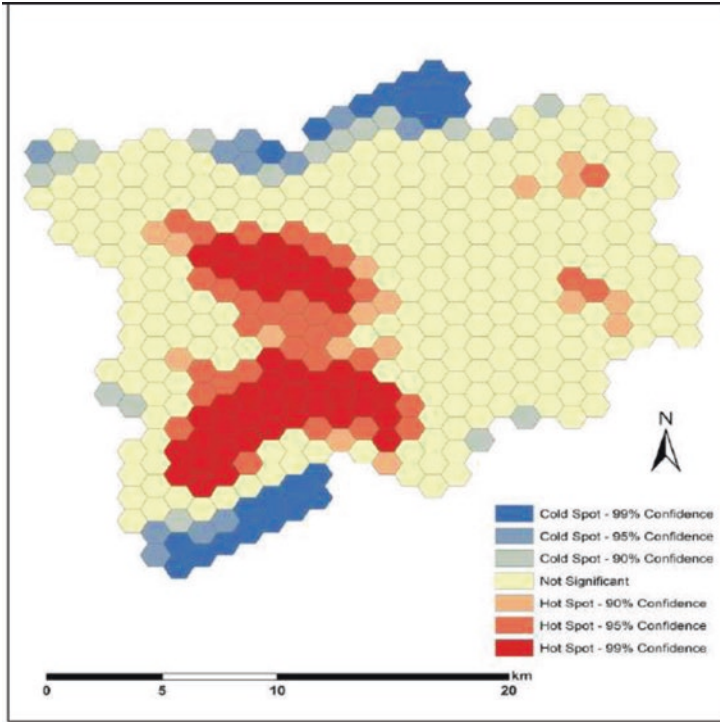


Fig. 7.7 GGHNP lightning strike density showing hot and cold spots

7.5.2 Hotspot Analysis Getis–Ord G_i^*

The map of Hotspot Analysis Getis–Ord G_i^* statistic using the 11-year lightning activity is presented in Fig. 7.7. It illustrates the regions of a statistically significant cluster of high and low values (hot and cold spots) presented in shades of red and blue based on the calculated Z-score and p-values. From Fig. 7.7, the main clusters are large and are identified as hot spots. These are at a higher elevation within the park such as in the south-western through the north-western and eastern part of the park. These hotspot areas cover 23.76% of the study area. Clusters of statistically significant low values or cold spots are mainly located in the northern part of the park. While 13.43% was found as statistically significant and identified as a cluster of low values (cold spot).

The results of the Getis–Ord G_i^* statistic for aggregated monthly data are revealed in Fig. 7.8. It showed that July and August (winter months) have a smaller area of coverage of high values of clustering and non-existing low values of clustering. Large coverage is identified as clusters of high values for all months between September and June. Table 7.2 showed the percentage of the area identified as clusters of high values (hotspot) and low values (cold spot), as well as non-significant

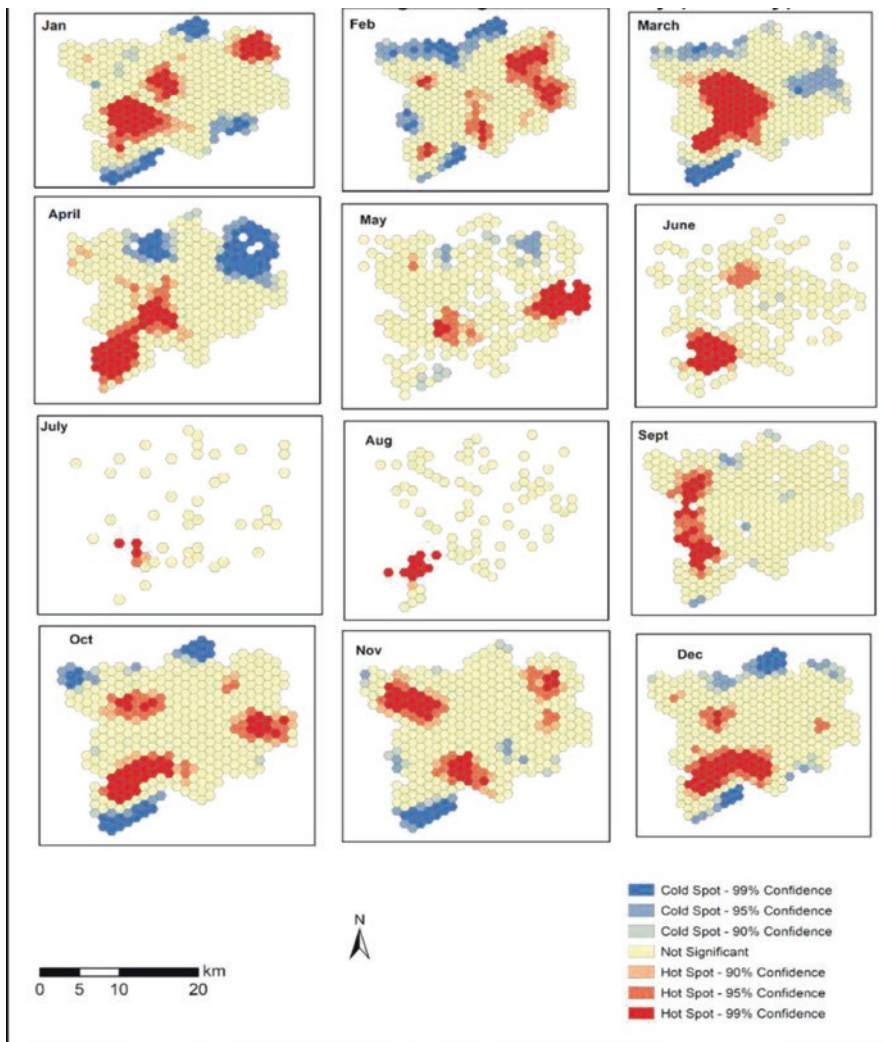


Fig. 7.8 GGHP monthly lightning strike density showing hot and cold spots

for the monthly dataset. February and March have the largest coverage identified as clusters of high values (hotspot). During winter months when the lightning activity is at least, the largest area of coverage of hotspot is located in June (18.27%) followed by August (12.38%) and July (10.36%) and located in the south-western part of the park and a small portion at the centre of the park.

During summer months when lightning activity is at its peak, the largest areas of coverage of hotspots are observed in February (23.70%) located in north-east and eastern parts of the park, followed by January (23.21%) and December showing the least (19.36%) and concentrated more in the south-west part of the park. During the autumn season, March (23.70%) contributed the highest area of coverage of hotspot

Table 7.2 Summary of monthly Getis–Ord G_i^* result showing the percentage of area identified as clusters of high values (hotspot), low values (cold spot), and non-significant

Month	High	Low	Non-Significant	Month	High	Low	Non-significant
Jan	23.21	13.03	63.76	Jul	10.36	0	89.64
Feb	23.7	18.86	57.44	Aug	12.38	0	87.62
Mar	23.7	23.25	53.05	Sept	14.75	3.64	81.62
Apr	19.32	19.91	60.77	Oct	21.6	10.99	67.41
May	15.43	7.12	77.44	Nov	21.4	9.24	69.62
Jun	18.27	0.96	80.77	Dec	19.36	13.43	67.21
All	23.76	12.85	63.4				

located extremely at the central part followed by April (19.32%) located in south-western and May (15.43%) located in the eastern part of the park. The high values of the cluster during the spring season are high in October (21.60%) concentrated mostly in the south-western region and less in the eastern part of the park and followed by November (21.14%) located in the north-west portion, September with the least (14.75%) in north and south-western part of the park. The cold spots of lightning strike density are large in coverage during April and non-exist in July and August.

The hotspot coverage appears to be at its greatest during 22:00 SAST (30.08%), 03:00 SAST (26.19%) and 17:00 SAST (25.75%) as shown in Fig. 7.9 and Table 7.3. The north-western, south-western, and central mountains have a consistently high level of hotspot during these time periods and through 06:00 SAST (3.33%) where it is almost non-existence. In the mountains of north-eastern and eastern GGHNP, the hotspot coverage in this region of the park is consistent but relatively smaller in coverage expect during 01:00, 04:00, 12:00, 16:00, and 19:00 SAST. Cold spot coverage appears to be at its greatest during 03:00 SAST (38.11%) and occurs mostly over the north-eastern flat terrain region of GGHNP. Therefore, the results of the Getis–Ord G_i^* test reveal localized hot and cold spots of CG lightning activity within GGHNP and vary with the seasons on the monthly time scale as well as diurnally hour of the day. The hot spots are generally located in or near the mountains while most of the cold spots are located in the flat terrain of GGHNP.

7.5.3 Development of Lightning Hazard Map

The development of LHM was drawn from the Z-score of Hotspot analysis, interpolated, normalized, and classified according to the potential of lightning hazard. The map showing coverage extent of hazard severity is illustrated in Fig. 7.10. It revealed that 48.76% of the entire landmass of the GGHNP falls under the severe danger zone. Two patches of the extreme danger zone are seen on the map towards the southwestern part and north-central portion of the map. Only very few portions of the entire landmass fall under almost danger-free zone, suggesting that the entire landmass of the GGHNP is largely prone to lightning hazard (Fig. 7.11).

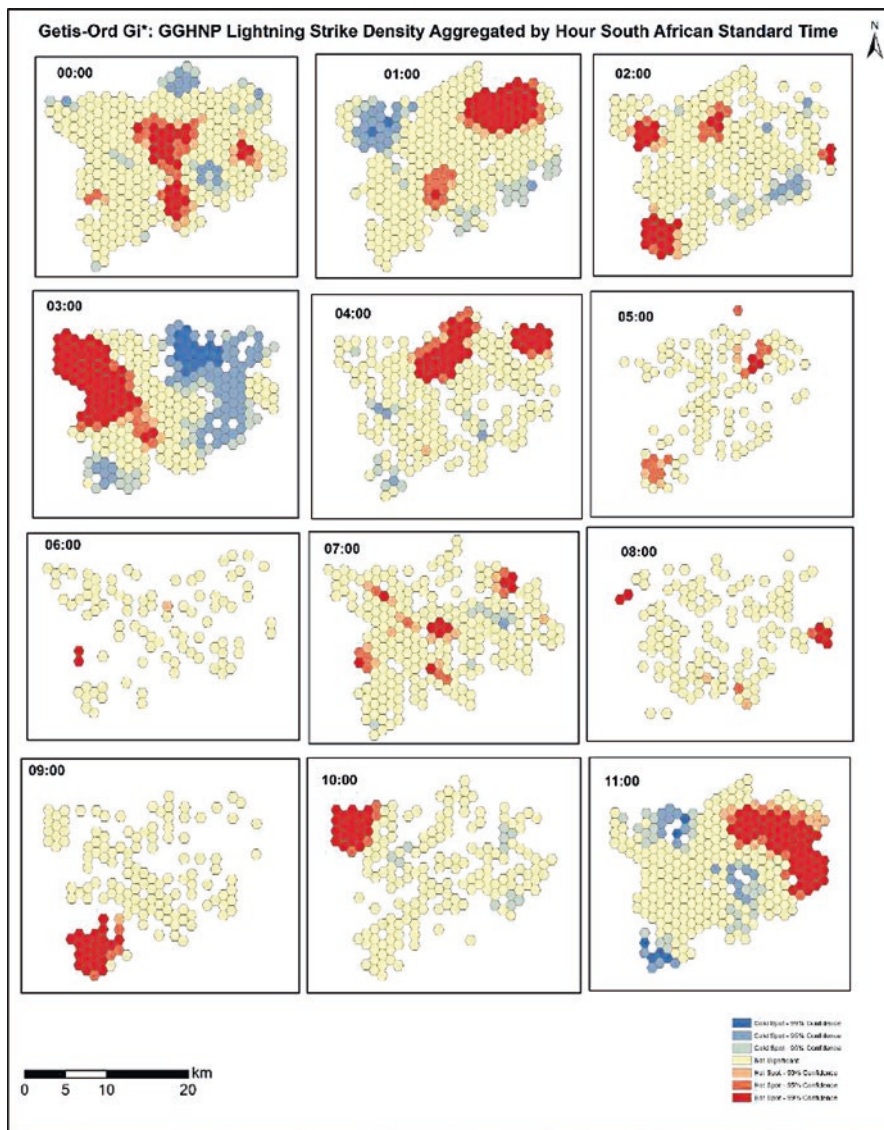


Fig. 7.9 GGHNPs average hourly lightning strike density showing hot and cold spots

7.5.4 Regression Analysis

In order to explore the relationship between the developed LHM and the terrain parameters (aspect, slope, and elevation), vegetation type, and fire scars, the regression analysis was executed. OLS regression (Table 7.4) yielded a model that explained 77% of the variation in lightning hazard map as explained by R^2 value of

Table 7.3 Summary of hourly Getis–Ord G_i^* result showing the percentage of area identified as clusters of high values (hotspot), low values (cold spot), and non-significant

Hour	High	Low	Non-significant	Hour	High	Low	Non-significant
00	18	10.25	71.75	12	22.14	22.43	55.47
01	18.14	15.61	66.25	13	12.51	9.26	78.22
02	16.03	7.77	76.2	14	24.46	20	55.54
03	26.19	38.11	35.69	15	22.25	8.33	69.4
04	21.32	5.98	72.7	16	23.03	18.9	58.06
05	16.39	0	83.61	17	25.75	21.24	53.75
06	3.33	0	96.6	18	20.86	14.98	64.16
07	13.56	3.71	82.73	19	18	15.99	66.01
08	7.8	0	92.2	20	16.17	8.55	75.28
09	17.61	0	82.39	21	22.25	14.09	63.77
10	12.6	6	81.4	22	30.08	13.29	56.63
11	23.4	17.08	59.52	23	19.1	12.62	68.28

0.77. The coefficient statistic which explains the type and strength of co-relationship showed negative relationship between LHM and aspect (-0.0424). However, positive and statistically significant relationship was found on fire scars (4.5668), slope (0.683), vegetation (0.021), and elevation (0.0029). These results are in agreement with the study conducted in Yellowstone National Park (Amrhein, 2017), whereby there was no relation of any aspect with lightning activity. The predictor variables used to predict spatial clustering all have variable inflation factor (VIF) less than 7.5 (Table 7.4) indicating little redundancy amongst variables except fire scars. However, fire scars have a robust relation with LHM.

The model was identified as statistically significant owing to the very low value of Joint F- and Wald-Statistic that is smaller than 0.05. With the Koenker (BP) statistics showing no statistical significance indicate that the model is consistent in data space, the variation in the relationship between predicted lightning strike density and explanatory variables does not change within explanatory variable magnitude. Therefore, there is no heteroscedasticity (non-constant variable or non-stationary) in the model. The Jarque–Bera Statistic test was also not statistically significant indicating that the regression residuals are normally distributed with a p-value higher than 0.05, therefore the model is unbiased. The adjusted R^2 and AICs values of the model are 0.63 and 73.66, respectively, validating the sound performance of the predicted model.

7.6 Discussion

The study revealed the outcomes in assessing the spatio-temporal patterns of CG lightning activity over the GGHNP. The application of statistical spatial autocorrelation and clustering techniques such as Global Moran I and Getis–Ord G_i^* was

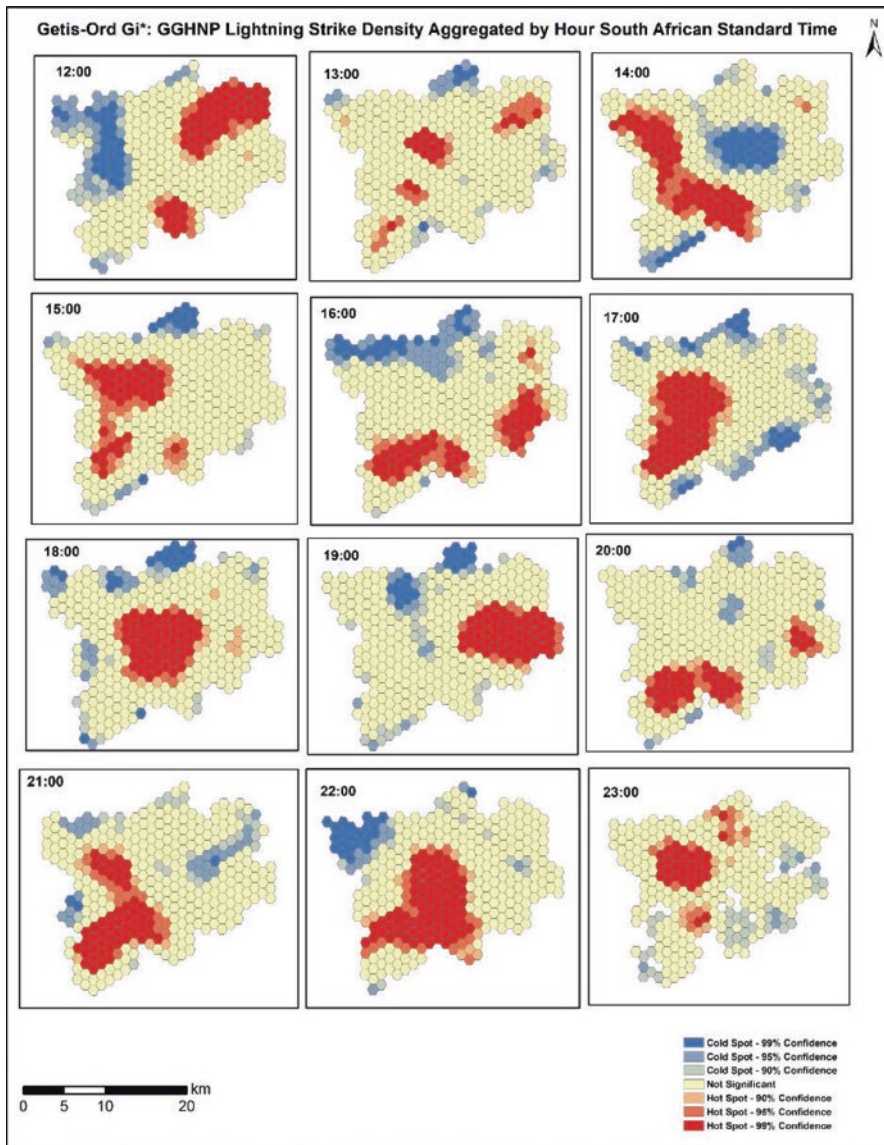


Fig. 7.10 GGHNP average hourly lightning strike density showing hot and cold spots (contd)

effective in delineating the LHM, identifying what areas of the park experience clusters of lightning activity. The regression analysis was performed testing the relationship between the developed LHM and physical properties of GGHNP terrain.

The monthly strike count increases from the minimum value in July (0.08%) and displays a peak in December (23.80%) as shown in Table 7.1. It is observed that the maximum lightning strikes count occurred in the summer months (DJF), accounting

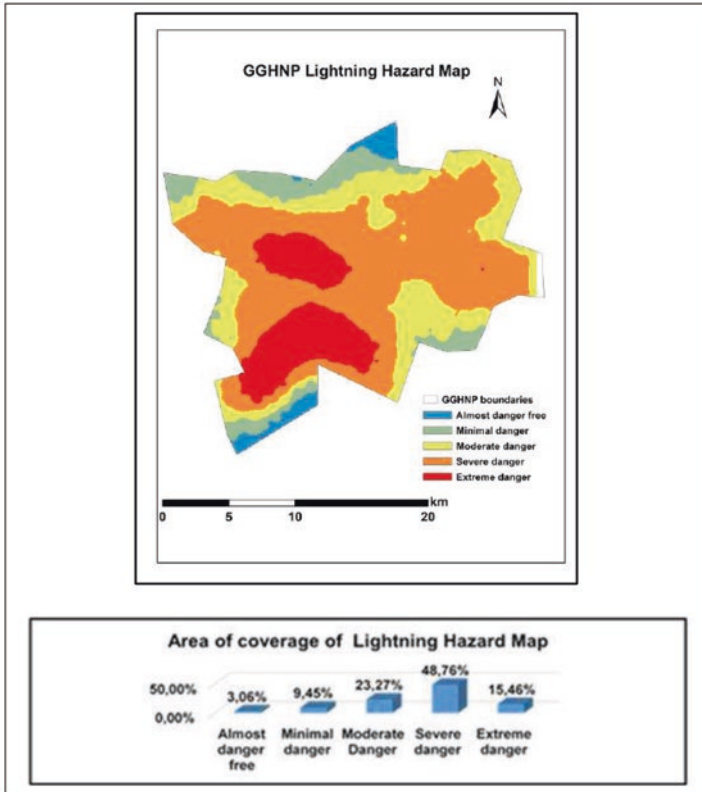


Fig. 7.11 Lightning hazard map for GGHNP (2007–2017) showing coverage extent of hazard severity

Table 7.4 OLS regression diagnostic for the entire dataset

Dependent variable	Lightning hazard map					
Variables	Coefficient	Std. error	t-Statistic	Probability	Robust_Pr	VIF
Aspect	-0.0424	0.0606	-0.6949	0.4970	0.4884	1.41
Elevation	0.0029	0.0008	3.5989	0.0024*	0.0003*	2.14
Slope	0.0683	0.0699	0.9773	0.3429	0.2706	1.72
Vegetation	0.0211	0.0676	0.3125	0.7586	0.6393	1.35
Fire	4.5668	6.1007	0.74857	0.4649	0.008631*	37.164
R-Squared	0.770884	Wald-Statistic	0.000000*			
Adjusted R-Squared	0.670646	Koenker (BP)	0.415350			
(AICc)	73.663751	Jarque-Bera	0.789538			
F-Statistic	0.000382*					

for 56.26% of the total lightning strikes. This is followed at a distance by the spring (SON) and autumn (MAM) months. SON and MAN accounted for 28.84% and (14.22%), respectively, with the lowest count in the winter (JJF) months (0.68%). Also, we observed that as the winter season progresses, that is April upwards, lightning strikes count showed a decreasing trend. This decreasing trend during the autumn season moving into the winter season is constituent with Dewan et al. (2018) who reported a shift in lightning strikes count with the change in season in Bangladesh. The summer peaks and the consistent monthly variability are consistent with Bhavika (2007) and Mayet et al. (2016). The lightning strikes observed during summer months are associated with the nature of the terrain leading to orographic forcing; the increase in the total precipitable water column as a result of abundant moisture in the atmosphere; an increased surface temperature due to intense solar heating leading. The persistent heating of the land atmosphere creates instability in the atmosphere, by enhancing convection activities leading to severe storms heralded by lightning.

The average diurnal variation (2007–2017) as depicted in Fig. 7.3 suggests that lightning is more prevalent in terms of occurrence from 14:00 to 18:00 SAST with two clear maxima at 15:00 SAST and 17:00 SAST. The lowest lightning activity is during the morning hours at 05:00 and 06:00 SAST, and yet again at hour 08:00 SAST. A 24-h distribution of lightning activity was divided by 6-h periods revealed the following pattern: early mornings (00–05:59) 7.82%, late morning (06:00–11:59) 3.72%, afternoon (12:00–17:59) 55.60%, and evening (18:00–23:59) 32%. From the foregoing, within the GGHNP, the lightning activity follows an afternoon–evening maxima. A comparison of diurnal variation across the seasons reveals that lightning activity is predominantly late afternoon-type, although it is not evident in the winter season. Both summer and autumn have prominent peak at 17:00 SAST and spring at 15:00 SAST. During winter, lightning activity is greatly diminished, however, there is a prominent peak at 02:00 SAST. The diurnal variability and inter-seasonal diurnal variability observed in Figs. 7.3 and 7.4 are in agreement with the study by Dewan et al. (2018), which found that peak lightning activity usually occurs during the afternoon–evening hour.

Number of factors may be related to this type of diurnal variation; these include diurnal solar cycle leading to destabilisation of the atmosphere and development of convective particular in springs and summer seasons (Williams, 1994). In south-western and north-central part of GGHNP, topography forcing the Thaba Bosiu Plateau and the foothills of Maluti Mountains allow convection and associate lightning to develop. Thus, topography in conjunction with synoptic system may lead to convective development (Qie et al., 2003) subsequently to the development of thunderstorm and lightning. Early morning peaks observed in winter season might be attributed to land and sea breezes circulation, nocturnal valley wind which promotes convection to early mornings and vertical wind shear for local convection (Dewan et al., 2018).

Regional road that passes through the GGHNP may enhance aerosol in atmosphere caused by increased anthropogenic activities within and adjacent to the park. The study by Mushtaq et al. (2018) showed that presence of aerosol in the

atmosphere may affect the lightning activity. South-western and northern central part of GGHNP support the notion that mesoscale convective is higher in the mountainous area. Qie et al. (2003) articulated three trigger mechanisms of such concept as orographic and terrain effects, presence of wind discontinuity line or dry line, and availability of vegetation moisture. Since these areas of the park are dominated by moderate height terrain, orographic lifting with respect to complex terrain could initiate conditional instability of atmosphere which favours the development of thunderstorm – facilitated lightning. Therefore, these mechanisms influence the spatial clustering of lightning activity over the study area.

Spatial autocorrelation analysis revealed that the clustering of lightning strikes at the park is at a distance of about 1.2 km. This connotes that strikes clustered with other strikes are not likely to strike an individual specific location from centre of cluster of strikes much beyond a circle with radius of 1.2 km. Spatial regression analysis (OLS) identified that elevation, slope, vegetation type, and fire scars are as statistically significant and positive in predicting the development of LHR. The vegetation-type variable was statistically significant showing a positive relation with LHM. This relation of vegetation type with LHM could be viewed in light of the vegetation of the study area. GGHNP is predominantly an Afromontane grassland park. There is a conjecture that grassland has much higher sensible heat flux because they have senesced during dry season, and an increased sensible heat flux may drive thermal convection and increase lightning activity. Although fire scars were found to be the only variable with the highest IVF values, which is responsible for multicollinearity and the most variables with the robust relationship with the LHM. This multicollinearity is due to the fact that the short-period dataset (1 year dataset) was used for this variable; therefore, increasing the sample size or long-period dataset could be a solution (ArcGIS, 2013). A small fire scar will show an increase in heating, but its impact on the heating of the boundary layer will be minimal (Kilinc and Beringer, 2007).

7.7 Conclusion

To the best of our knowledge, this is the first study of its kind to make use of SALDN data over the mountainous protected area to explore the statistical spatial and temporal patterns of lightning activity: the first to employ spatial analysis techniques to determine the clustering of CG lightning within the GGHNP. Global clustering spatial pattern was calculated using Global Moran/employed on lightning-strike for the entire dataset (2007–2017), and monthly and hourly data revealed that there is strong evidence of global clustering and spatial patterns are statistical spatially significant and appear to be clustered except in July, late morning hour of 06:00, 08:00, and 09:00 SAST. The study demonstrated that the overall spatial pattern of CG lightning activity varies with time due to regional and local weather patterns as influenced by a large scale of climatic nodes (ENSO and SAM). This relationship still needs to be explored. Monthly variation revealed that lightning activities are at

peak during summer, in December, while diurnal variation revealed afternoon-evening maxima attributed to orographic effect, availability of abundant moisture, and diurnal solar heating cycle. The developed LHM revealed that almost 16% of the study area is at risk of lightning. OLS helped to identify the key factors contributing to the lightning threat being elevation. The study is a step towards new information regarding the spatio-temporal distribution of CG lightning. The data derived from this study would be of significance for wildfire models used to predict, monitor, and assess the lightning-induced wildfire. Knowing where and when lightning is mostly to cluster will allow managers to preposition suppression, plan for fuel treatment, and prepare fire prevention and public safety (Van Wagendonk and Cayan, 2008). Although this study furnished some initial results, incorporating strikes characteristics (polarity, multiplicity, and strength), regional climate conditions and local weather patterns that result from physical geography of GGHP would advance the understanding of spatio-temporal distribution of CG lightning activity. Knowledge of why positive or negative clusters occur in the study area can be used to improve lightning-induced wildfire models.

References

- Adelabu, S. A., Adepoju, K. A., & Mofokeng, O. D. (2018). Estimation of fire potential index in mountainous protected region using remote sensing. *Geocarto International*, 35, 29–46.
- Amrhein, E. (2017). *The geography of cloud-to-ground lightning in Yellowstone National Park*.
- Anderson, G., & Klugmann, D. (2014). A European lightning density analysis using 5 years of ATDnet data. *Natural Hazards and Earth System Sciences*, 14, 815–829.
- ArcGIS, Environmental Systems Research Institute (ESRI). (2013). *10.2 Desktop Help*. ESRI, Inc. Redlands, CA.
- Bentley, M. L., & Stallins, J. (2005). Climatology of cloud-to-ground lightning in Georgia, USA, 1992–2003. *International Journal of Climatology: A Journal of the Royal Meteorological Society*, 25, 1979–1996.
- Bhavika, B. (2007). *The influence of terrain elevation on lightning density in South Africa*. University of Johannesburg.
- Blumenthal, R., Trengrove, E., Jandrell, I. R. & Saayman, G. (2012). *Lightning medicine in South Africa*.
- Carr, D. B., Olsen, A. R., & White, D. (1992). Hexagon mosaic maps for display of univariate and bivariate geographical data. *Cartography and Geographic Information Systems*, 19, 228–236.
- Cecil, D. J., Buechler, D. E., & Blakeslee, R. J. (2014). Gridded lightning climatology from TRMM-LIS and OTD: Dataset description. *Atmospheric Research*, 135, 404–414.
- Cha, D., Wang, X., & Kim, J. W. (2017). Assessing lightning and wildfire hazard by land properties and cloud to ground lightning data with association rule mining in Alberta, Canada. *Sensors*, 17, 2413.
- Christian, H. J., Blakeslee, R. J., Boccippio, D. J., Boeck, W. L., Buechler, D. E., Driscoll, K. T., Goodman, S. J., Hall, J. M., Koshak, W. J., & Mach, D. M. (2003). Global frequency and distribution of lightning as observed from space by the Optical Transient Detector. *Journal of Geophysical Research: Atmospheres*, 108, ACL 4-1–ACL 4-15.
- Chuvieco, E., Aguado, I., Jurdao, S., Pettinari, M., Yebra, M., Salas, J., Hantson, S., De La Riva, J., Ibarra, P., & Rodrigues, M. (2014). Integrating geospatial information into fire risk assessment. *International Journal of Wildland Fire*, 23, 606–619.

- Chuvieco, E., Aguado, I., Yebra, M., Nieto, H., Salas, J., Martín, M. P., Vilar, L., Martínez, J., Martín, S. P. I., De La Riva, J., Baeza, J., Rodríguez, F., Molina, J. R., Herrera, M. A., & Zamora, R. (2010). Development of framework for fire risk assessment using remote sensing and geographic information system technologies. *Ecological Modelling*, *1*, 46–58.
- Dewan, A., Ongee, E. T., Rahman, M. M., Mahmood, R., & Yamane, Y. (2018). Spatial and temporal analysis of a 17-year lightning climatology over Bangladesh with LIS data. *Theoretical and Applied Climatology*, *134*, 347–362.
- Dissing, D., & Verbyla, D. L. (2003). Spatial patterns of lightning strikes in interior Alaska and their relations to elevation and vegetation. *Canadian Journal of Forest Research*, *33*(5), 770.
- Dowdy, A. J. (2016). Seasonal forecasting of lightning and thunderstorm activity in tropical and temperate regions of the world. *Scientific Reports*, *6*, 20874.
- Durrheim, G. (2010). *Monitoring for sustainable indigenous forest management in the Garden Route National Park*. Scientific Services, South African National Parks.
- Eskandari, S., & Chuvieco, E. (2015). Fire danger assessment in Iran based on geospatial information. *International Journal of Applied Earth Observation and Geoinformation*, *42*, 57–64.
- Evert, C. & Gijben, M. (2017). Official South African Lightning Ground Flash Density Map 2006 to 2017. Inaugural Earthing Africa Symposium and Exhibition, Thaba Eco Hotel, Johannesburg, 5-9.
- Evert, R., & Schulze, G. (2005). Impact of a new lightning detection and location system in South Africa. *2005 IEEE Power Engineering Society Inaugural Conference and Exposition in Africa*, 356–363.
- Frost, P., Kleyn, L., van den Dool, R., Burgess, M., Vhengani, L., Steenkamp, K. & Wessels, K. (2018). *The Elandskraal Fire, Knysna*. CSIR Report, (271960-1).
- Genton, M. G., Butry, D. T., Gumpertz, M. L., & Prestemon, J. P. (2006). Spatio-temporal analysis of wildfire ignitions in the St Johns River water management district, Florida. *International Journal of Wildland Fire*, *15*(1), 87–97.
- Getis, A., & Ord, J. K. (1992). The analysis of spatial association by use of distance statistics. *Geographical Analysis*, *24*, 189–206.
- Gijben, M. (2012). The lightning climatology of South Africa. *South African Journal of Science*, *108*, 44–53.
- Gijben, M., Dyson, L. L., & Loots, M. T. (2017). A Statistical scheme to forecast the Daily Lightning threat over Southern Africa using the unified model. *Atmospheric Research*, *194*, 78–88.
- Gill, T. (2009). *Initial steps in the development of a comprehensive lightning climatology of South Africa*. Doctoral dissertation, University of the Witwatersrand.
- Govender, N. (2011). *Proposed changes to the fire management policy of Golden Gate Highlands National Park*. South African National Parks. (SANP), Pretoria, RSA.
- Guha, A., Banik, T., Roy, R., & de Kumar, B. (2017). The effect of El Nino and La Nina on lightning activity: Its relation with meteorological and cloud microphysical parameters. *Natural Hazards*, *85*, 403–424.
- Huang, Y., Wu, S., & Kaplan, J. O. (2015). Sensitivity of global wildfire occurrences to various factors in the context of global change. *Atmospheric Environment*, *121*, 86–92.
- Javor, V., Stoimenov, L., Džaković, N., Dinkić, N., Javor, D., & Betz, H.-D. (2018). LINETGIS analysis of lightning flash density in Serbia based on ten years data. *Serbian Journal of Electrical Engineering*, *15*, 201–211.
- Kigotsi, J. K., Soula, S., & Georgis, J.-F. (2018). Comparison of lightning activity in the two most active areas of the Congo Basin. *Natural Hazards and Earth System Sciences*, *18*, 479–489.
- Killinc, M., & Beringer, J. (2007). The spatial and temporal distribution of lightning strikes and their relationship with vegetation type, elevation, and fire scars in the Northern Territory. *Journal of Climate*, *20*, 1161–1173.
- Kotroni, V., & Lagouvardos, K. (2008). Lightning occurrence in relation with elevation, terrain slope, and vegetation cover in the Mediterranean. *Journal of Geophysical Research: Atmospheres*, *113*.
- Mariani, M., Fletcher, M. S., Holz, A., & Nyman, P. (2016). ENSO controls interannual fire activity in southeast Australia. *Geophysical Research Letters*, *43*, 10,891.

- Mayet, N., Knight, J., & Grab, S. W. (2016). Spatial and temporal patterns of lightning strikes in the eastern Lesotho Highlands, southern Africa. *South African Geographical Journal*, 98, 321–336.
- Moran, P. A. (1950). Notes on continuous stochastic phenomena. *Biometrika*, 37, 17–23.
- Mushtaq, F., Lala, M. G. N., & Anand, A. (2018). Spatio-temporal variability of lightning activity over J&K region and its relationship with topography, vegetation cover, and absorbing aerosol index (AAI). *Journal of Atmospheric and Solar-Terrestrial Physics*, 179, 281–292.
- Price, C., & Federmesser, B. (2006). Lightning-rainfall relationships in Mediterranean winter thunderstorms. *Geophysical Research Letters*, 33, L07813.
- Qie, X., Toumi, R., & Yuan, T. (2003). Lightning activities on the Tibetan Plateau as observed by the lightning imaging sensor. *Journal of Geophysical Research: Atmospheres*, 108.
- Rakov, V. A., & Uman, M. A. (2003). *Lightning: Physics and effects*. Cambridge University Press.
- South African National Parks, S. (2013). *Golden Gate Highland National Park Management Plan 2013–2023*. Access on 01 February 2018. https://www.sanparks.org/assets/docs/conservation/park_man/golden-gate-draft-plan.pdf
- Strydom, S., & Savage, M. J. (2016). A spatio-temporal analysis of fires in South Africa. *South African Journal of Science*, 112, 1–8.
- Van Wagtenonk, J. W., & Cayan, D. R. (2008). Temporal and spatial distribution of lightning strikes in California in relation to large-scale weather patterns. *Fire Ecology*, 4, 34–56.
- Williams, E. R. (1994). Global circuit response to seasonal variations in global surface air temperature. *Monthly Weather Review*, 122, 1917–1929.